HHS Public Access

Author manuscript

Magn Reson Med. Author manuscript; available in PMC 2017 March 01.

Published in final edited form as:

Magn Reson Med. 2016 March ; 75(3): 1333–1340. doi:10.1002/mrm.25562.

Comparison of Muscle BOLD Responses to Arterial Occlusion at 3T and 7T

Theodore F. Towse[1,2,3], **Benjamin T. Childs**[1], **Shea A. Sabin**[1], **Emily C. Bush**[1], **Christopher P. Elder**[1], and **Bruce M. Damon**[1,3,4,5]

[1]Institute of Imaging Science

[2]Department of Physical Medicine and Rehabilitation

[3]Department of Radiology and Radiological Sciences

[4]Department of Biomedical Engineering

[5]Department of Molecular Physiology and Biophysics

Abstract

Purpose—The purpose of this study was to determine the feasibility of muscle BOLD (mBOLD) imaging at 7T by comparing the changes in R_2* of muscle at 3 and 7T in response to a brief period of tourniquet-induced ischemia.

Methods—Eight subjects (3 male), aged 29.5 ± 6.1 years (mean ± standard deviation, SD), 167.0 ± 10.6 cm tall with a body mass of 62.0 ± 18.0 kg, participated in the study. Subjects reported to the lab on four separate occasions including a habituation session, two MRI scans, and in a subset of subjects, a session during which changes in blood flow and blood oxygenation were quantified using Doppler ultrasound (U/S) and near-infrared spectroscopy (NIRS) respectively. For statistical comparisons between 3T and 7T, R_2* rate constants were calculated as $R_2^* = 1/T_2^*$.

Results—The mean pre-occlusion R_2* value was greater at 7T than at 3T (60.16 ± 2.95 vs 35.17 ± 0.35 s^{-1} respectively, p <0.001). Also, the mean $\Delta R_2^*_{END}$ and $\Delta R_2^*_{POST}$ values were greater for 7T than for 3T (−2.36 ± 0.25 vs. −1.24 ± 0.39 s^{-1}, respectively, Table 1).

Conclusion—Muscle BOLD contrast at 7T is as much as six-fold greater than at 3T. In addition to providing greater SNR and CNR, 7T mBOLD studies may offer further advantages in the form of greater sensitivity to pathological changes in the muscle microcirculation.

Keywords

NIRS; Doppler ultrasound; transverse relaxation; human; ultra-high field MRI

INTRODUCTION

Blood oxygenation-level dependent (BOLD) contrast in skeletal muscle was first described more than 15 years ago [1–3]. Since that time, the applications of muscle BOLD (mBOLD)

Address for correspondence: Bruce M. Damon, PhD, AA-1105 MCN, 1161 21st Ave S, Nashville, TN USA 37232, bruce.damon@vanderbilt.edu, Phone: (615) 322-8355, Fax: (615) 322-0734.

contrast have been advanced in several ways. For example, function-based mBOLD contrast has been used to infer small vessel function following isometric contractions [4–8], arterial occlusion in patients with peripheral artery disease patients [9], and the infusion of vasoactive compounds [10]. Also, the dependence of the rate of RF-reversible dephasing on blood deoxyhemoglobin content has allowed the use of mBOLD-based methods to estimate blood O_2 extraction during exercise [11,12]. Therefore, mBOLD contrast is extremely useful for studying skeletal muscle physiology and pathophysiology.

Like BOLD contrast in other organs, the mechanisms of BOLD contrast in skeletal muscle may operate through intravascular (IV) and/or extravascular (EV) relaxation mechanisms. Intravascular BOLD contrast refers to the effects of hemoglobin content and oxygen saturation on the relaxation of intravascular spins, while EV BOLD contrast refers to the effects of hemoglobin content and oxygen saturation on the relaxation of extravascular spins. However, a salient difference between BOLD contrast in skeletal muscle and organs such as the brain is the vascular structure. While brain capillaries may be considered to be a collection of randomly oriented structures, more than 90% of capillary length is parallel to the muscle fibers [13,14]. Typical subject positioning in the MRI system causes muscle blood vessels to lie generally parallel to B_0. Because the EV BOLD effect depends partly on the angle formed by the blood vessels and B_0, modeling studies have predicted that the EV mBOLD effect would be very small at B_0 field strengths of 3T and below [4,10,15]. This hypothesis was tested experimentally in the tibialis anterior muscle and found to be tenable for typical leg positions and muscle fiber orientations [16]. Consequently, mBOLD-dependent relaxation effects or contrast changes from 3T or below can be interpreted with respect to IV contrast mechanisms only.

When compared to studies at lower field strength, mBOLD studies at ultra-high fields may differ in several fundamental ways. One advantage to 7T MRI is an improved signal-to-noise ratio (SNR) due to greater spin polarization, which may be used in imaging studies to improve spatial and/or temporal resolution. Another potential advantage is improved contrast, including an improved contrast-to-noise ratio (CNR) and/or new or more physiologically specific sources of contrast. In particular, the rapid transverse relaxation of blood at 7T [17] is expected to favor EV BOLD contrast. A final general advantage is improved SNR and spectral dispersion for MR spectroscopy studies. These possibilities have promoted the use of 7T MRI for studies of human brain structure and function. However, during this same period, there have been very few musculoskeletal MRI studies at 7T and even fewer have been dedicated to skeletal muscle [18–22].

Presuming that the difficulties associated with ultra-high field MRI studies of skeletal muscle can be successfully overcome, ultra-high field MRI may afford distinct advantages for mBOLD studies. As an initial step toward this goal, and to test the hypothesis that the magnitude of mBOLD-dependent responses would be greater at 7T than at 3T, we studied the responses of the effective transverse relaxation time constant (T_2*) to proximal arterial occlusion at 3T and 7T. To provide an enhanced physiological context with which to interpret these data, we further obtained Doppler ultrasound (U/S) measures of blood flow and near infrared spectroscopy (NIRS) measures of oxyhemoglobin saturation (%HbO_2) and

total hemoglobin concentration ([THb]) as well. The outcome of this study supports the continued development of mBOLD methods for 7T.

METHODS

Subjects and Testing Protocol

Eight subjects (3 male), aged 29.5 ± 6.1 years (mean ± standard deviation, SD), 167.0 ± 10.6 cm tall with a body mass of 62.0 ± 18.0 kg, participated in the study. Their mean systolic and diastolic blood pressures were 114 ± 10 and 66 ± 8 mmHg, respectively. All subjects gave written informed consent in accordance with the Institutional Review Board prior to participation. All subjects were free from physician-diagnosed chronic disease with an ankle brachial index (ABI) greater than 1.0 (1.08 ± 0.12).

Subjects reported to the lab on four separate occasions. Visits were scheduled at approximately the same time of day (± 1 hr) and each visit was separated by at least 1 week. To limit the influence of diet and exercise on study outcome variables, subjects were asked to refrain from: 1) vigorous exercise for at least 24 hours prior to the testing; 2) consuming caffeinated food or beverages for at least 6 hours prior to testing; and 3) taking any over-the-counter medication 24 hours prior to each testing session. A pre-test questionnaire was completed by each subject prior to testing to confirm compliance with pre-test conditions. Any subject not in compliance was rescheduled for testing at a later date.

On the initial visit, the subjects read and signed the informed consent document and completed a health-history questionnaire and a magnetic materials safety screening form. In addition, each subject's height and weight were measured and recorded. The subject then rested quietly on a patient table for 15 minutes after which time his/her blood pressure was measured in the brachial artery using a standard arm blood pressure cuff and a sphygmomanometer. Blood pressure in the posterior tibial artery was measured using a leg blood pressure cuff and a portable hand-held U/S device (Nicolet, Elite Model 200, Madison WI). The ABI was calculated as the ratio of systolic blood pressure (mmHg) in the posterior tibial artery to the systolic blood pressure in the brachial artery. Experimental days 2 and 3 included MRI scans on either the 3 or 7 tesla system (in randomized block design). On experimental day 4, in a subset of subjects, changes in blood flow and blood oxygenation were quantified using U/S and NIRS respectively.

Reactive Hyperemia Protocol

A 24×122.5 cm^2, thigh-specific vascular cuff (Model CC22, Hokanson, Bellevue WA) was placed around the thigh proximal to the knee joint. The cuff was rapidly inflated (within ~1 s) to a pressure of 250 mmHg using a rapid cuff inflator (Model E20, Hokanson, Bellevue WA) and was maintained at this pressure for 5 minutes. This same reactive hyperemia protocol was implemented for all testing sessions (MRI, NIRS and U/S).

MRI Procedures

Subjects were positioned supine in the scanner with both legs extended. The subject's left leg was positioned at heart level and the largest portion of the left calf was centered in an

extremity coil. Padding was placed around the leg to allow the cuff to inflate and deflate without altering the position the leg in the coil. As an additional precaution against motion, the subject's leg was secured to the patient table using nylon straps with Velcro® closures. Care was taken to position the subject in the same manner for all testing sessions; the knee angle and the positions of the calf in the coil were measured and standardized across the visits. The location of the imaging slice was marked with a permanent marker and the position of this mark relative to the distal border of the patella was measured. This measurement was used to replicate the imaging at each field strength and the position of the NIRS probe head.

3T procedures—Images were acquired using a Philips Intera Achieva (Philips Healthcare), whole-body scanner and an 8-channel receive only knee coil. The quadrature-body coil was used for RF field transmission. High-resolution anatomical images (turbo spin-echo, FOV = 200×200 mm^2, 11 slices, 5 mm slice thickness, 3 mm gap) centered at mid-calf were acquired for planning purposes. Following localized shimming over the posterior muscle compartment of the leg, functional images were acquired continuously for 14 minutes (including 2 minutes of baseline, 5 minutes of ischemia, and 7 minutes of reactive hyperemia). The image acquisition/reconstruction parameters were: six-shot, multi-echo turbo field echo, echo-planar images (TFE-EPI) with *TR*=1000 ms, 15 echoes with minimum *TE*=4.43 ms and echo spacing=6.14 ms, acquisition matrix of 64×64 (reconstructed to 128×128), and a single 200×200 mm^2, 10 mm thick slice. At both 3T and 7T, cuff inflation and deflation were timed as nearly as possible to correspond to the time between the completion of one multi-shot image acquisition and the start of the subsequent one.

7T procedures—Scanning was performed on a Philips 7T scanner (Philips Healthcare) using a 3 element transmit/receive partial-volume extremity coil, which provided excellent coverage of the soleus and the medial and lateral heads of the gastrocnemius muscle. All images were acquired as near to the same anatomical location as in the 3T study as possible. High-resolution anatomical scans (turbo spin-echo, FOV = 200×200 mm^2, 11 slices, 5 mm slice thickness, 3 mm gap) were acquired for localization. A 3D ΔB_0 map was obtained using: *TR* = 9 ms, *TE*= 2.9/3.9 ms, a 200×200×75 mm^3 field of view with an 80×80×15 matrix. The ΔB_0 map was used to verify the performance of localized shimming in the posterior compartment. The functional imaging sequence was nearly identical to the sequence at 3T: six-shot, multi-echo TFE-EPI with *TR*=1000 ms, 15 echoes with minimum *TE*=4.32 ms and echo spacing=6.04 ms, an acquisition matrix of 64×64 (reconstructed to 128×128), and a single 200×200 mm^2, 10 mm thick slice. During pilot testing B_1 maps were acquired to ensure the appropriate flip angle was being achieved in the medial gastrocnemius.

MR images were analyzed in MATLAB (The MathWorks®, Natick MA) using custom written code. Regions of interest (ROIs) 2–3 cm^2 were drawn in the medial gastrocnemius muscle in the same anatomical location as the center of the NIR sampling volume. Care was taken when positioning the ROI to exclude connective tissue and resolved vessels. Images were inspected for motion on an individual basis and the ROI was repositioned as needed.

T_2* values were calculated from exponential fitting of the signal decay curve assuming a mono-exponential decay. For statistical comparisons between 3T and 7T, R_2* rate constants were calculated as $R_2^* = 1/T_2^*$. The data were characterized with the mean pre-occlusion value, the mean end-occlusion value (the average of the last 30 s of occlusion), and with the peak post-occlusion value ($R_2^*_{PRE}$, $R_2^*_{END}$, and $R_2^*_{POST}$, respectively). The differences of the end-ischemia and peak post-occlusion R_2* values from the pre-occlusion mean value ($\Delta R_2^*_{END}$ and $\Delta R_2^*_{POST}$, respectively) were calculated. Also, the time at which $R_2^*_{POST}$ occurred ($t_{R2^*,\,POST}$) was calculated.

U/S and NIRS Procedures

In addition to the MRI procedures, a subset of subjects completed simultaneous U/S and NIRS studies during arterial occlusion (n = 6). The positioning of the subject for this portion of the study was replicated as nearly as possible as that during the MRI portion of the study.

Ultrasound—Blood velocity data were acquired using an 8-MHz linear probe (Model 8L-RS) mounted to a portable U/S system (GE LOGIQ *e*, GE Medical Systems, Milwaukee WI). The U/S probe was positioned along the popliteal fossa to visualize the popliteal artery (PA). Interleaved brightness-mode (B-mode) and pulse wave-mode (PW-mode) images were acquired continuously from the PA. The sampling depth and gate were optimized for each subject to acquire velocity data from the center of a 2–3 mm region of the vessel. The probe was held securely in place and data were acquired at an insonation angle between 45 and 60°. Data were acquired in bins of 45-s cinematic (CINE) loops, stored and analyzed using software available on the GE LOGIQ *e* system. Blood flow was calculated by multiplying the cross-sectional area of the popliteal artery mean blood velocity over the duration of the pulse-waveform (time average mean, V_{TAMEAN}) according to the equation:

$$Blood\ Flow\,(\mathrm{ml/min}) = V_{TAMEAN}\,(\mathrm{cm/s}) \cdot \pi \cdot [PA\ diameter\,(\mathrm{cm})/2]^2 \cdot 60\,(\mathrm{s/min}) \quad [1]$$

Resting blood flow was calculated from the average of 10 velocity waveforms and 10 vessel diameter measurements. Vessel diameter measurements were made on the B-mode images at the end of diastole. The highest blood flow following the release of the arterial cuff is reported as the peak blood flow. However, on two occasions movement of the subject or the arterial cuff upon cuff deflation resulted in missing the first few seconds of reactive hyperemia and potentially the true peak.

Tissue-oxygenation data were collected using a frequency domain, multi-distance NIRS oximeter (Model 96208, ISS, Inc.) and its accompanying software as discussed in further detail previously [15]. The NIRS probe was positioned over the medial head of the gastrocnemius muscle, at the same anatomical location where the MR images were acquired during visits 2 and 3. The probe-head was secured to the leg using a nylon elastic strap with Velcro© closures. To limit contamination of the NIRS signal by ambient light, a black cloth was wrapped around the NIRS probe head and calf muscles of the leg. Prior to securing the NIRS probe-head to the skin the subjects skin was cleaned with a 70% isopropyl alcohol solution and the oximeter was calibrated using a muscle tissue-like phantom according to the

manufacturer's instructions. The $\%HbO_2$ and [THb] were determined using the manufacturer's algorithms.

Data were analyzed using MATLAB version 8.0.0.783. The raw data were sampled at 5.16 Hz and smoothed with a seven-point (1.37 s) moving average. Discreet analysis of the $\%HbO_2$ data consisted of calculating the average value over the final 12 s prior to occlusion and during the last 5 s of occlusion ($\%HbO_{2,PRE}$ and $\%HbO_{2,END}$, respectively); the corresponding values for [THb] were also calculated and are denoted with similar subscripts. The post-occlusion data were analyzed as continuous data by fitting them in a least squares manner to a sixth-order polynomial and recording the maximum post-occlusion value and the earliest time at which that value occurred ($\%HbO_{2,POST}$ and $[THb]_{POST}$, respectively).

Statistical Analysis

Data are presented as mean ± standard error. Tests of mean values at 3T vs. 7T were made using a paired Student's *t*-test. The significance of variables reflecting changes from pre-occlusion baseline was determined by forming 95% confidence intervals (95% CI's) around the mean value. Statistical significance was accepted at $p < 0.05$.

RESULTS

MRI Data

Figure 1 shows sample anatomical images obtained at 3T (panel A) and 7T (panel B). Consistent with the use of the partial volume coil, there is substantial signal dropout from the anterior compartment in the image obtained at 7T. The images also reflect the similarity of axial slice location within the leg in the two studies.

Sample T_2* curve-fitting results from the data obtained during the pre-occlusion period at 3T and 7T are provided in Figure 2. Sample T_2* maps for pre-occlusion, end-occlusion, and post-occlusion time points are shown in Figure 3. Sample R_2* time courses for 3T and 7T studies are shown in Figure 4. A ~50 s period of pre-occlusion data is shown. At the onset of occlusion, artifacts associated with cuff inflation are seen in the figure and marked by a dotted line. On occasion, application of the cuff resulted in a brief upward or downward spike in signal intensity, which quickly returned to baseline. The 5 minutes of cuff-induced ischemia caused the R_2* to increase slightly at 3T and to a greater extent at 7T. A rapid increase in R_2* occurred at 3T immediately after deflation of the cuff; this effect was not present at 7T likely. The mean values for R_2* at pre-occlusion, end-occlusion, and peak post-occlusion are shown in Table 1 for 3T and 7T. The mean pre-occlusion R_2* value was greater at 7T than at 3T ($p < 0.001$). Also, the mean $\Delta R_2{}^*_{END}$ and $\Delta R_2{}^*_{POST}$ values were greater for 7T than for 3T (Table 1). The average $t_{R2^*,\,POST}$ values for 3T and 7T are also given in Table 1.

U/S and NIRS Data

Figure 5 shows sample NIRS data. Both $\%HbO_2$ (panel A) and [THb] (panel B) decreased upon cuff inflation. Upon cuff release, both $\%HbO_2$ and [THb] recovered to and then transiently exceeded the pre-occlusion value. The group-mean data are found in Table 2.

Also indicated are the times at which the peak $\%HbO_2$ and [THb] responses occurred and the 95% CI's surrounding the $\Delta\%HbO_{2END}$ and $\Delta\%HbO_{2POST}$ mean values. The CI's indicate a significant decrease in $\%HbO_2$ to below the pre-occlusion mean value at end-occlusion and a significant increase in $\%HbO_2$ to above the pre-occlusion mean value during the post-occlusion period. Similar behaviors are noted for the group-mean [THb] data.

Figure 6 shows a sample color Doppler image, B-mode image of the vessel and a sample pulse waveform. Across all subjects, the mean pre-occlusion flow was 45.6 ± 14.6 ml/min. The mean peak post-occlusion flow was 535.6 ± 67.6 ml/min, a difference of more than 11-fold ($p < 0.001$). In four subjects, a distinct post-occlusion maximum was observed at an average post-occlusion time of 11.1 ± 2.6 s. A larger increase in blood flow during reactive hyperemia was associated with a larger increase in [THb] (r = 0.60) and a longer time-to-peak [THb] (r = −0.65).

DISCUSSION

In this study, we have described human muscle BOLD contrast at 7T, and we have compared the R_2* responses to a brief period of tourniquet-induced ischemia at 7T to those from 3T. This is the first such study of which we are aware. Below, we describe the attendant technical challenges to these studies, interpret the responses, and propose possible advantages of these studies for physiological characterization of skeletal muscle physiology and pathophysiology.

Technical Challenges to Skeletal Muscle Studies at 7T

Previous authors have described the technical challenges of ultra-high field MRI studies of skeletal muscle [18,19]. Among these, B_0 and B_1 inhomogeneities are well-recognized difficulties for human studies at ultra-high magnetic field strengths. In these studies, we used localized B_0 shimming routines over the posterior compartment of the leg to improve the field homogeneity in the medial gastroc (Figure 1C). Although the partial volume coil that we used had limited coverage for the entire cross-section of the calf, it provided high signal in the medial gastroc, as reflected by the image in Figure 1B and the high SNR of the T_2*-dependent signal decay data in Figure 2B. Furthermore, B_1 maps acquired during pilot testing were used to ensure a robust B_1 profile in the medial gastroc. Motion artifacts were controlled in the multi-shot functional imaging sequences by the use of padding and strapping to restrict subject motion and by timing the inflation and deflation of the arterial cuff events to fall between separate image acquisitions. Consequently, the multi-shot sequences were able to provide high quality images with very small echo spacing for robust characterizations of T_2*. Other challenges of ultra-high field studies include a general pattern of lengthening of T_1, shortening of T_2, and disproportionate shortening of T_2*; here, we show that the T_2* of skeletal muscle at 7T is ~17 ms (R_2* ~60 s^{-1}) at rest.

Physiological Responses to Arterial Occlusion

Proximal arterial occlusion is frequently used to study vascular physiology, pathology (e.g, [23–28]), and the biophysical basis of muscle BOLD contrast [4,11,13,14,22]. Here, we performed simultaneous U/S and NIRS studies of the responses to arterial occlusion. (We

note that in two subjects, it was not possible to obtain Doppler U/S data during the first few cardiac cycles following cuff release, so the comments pertaining to the arterial responses (vessel diameter, flow) pertain only to the remaining four subjects.) Consistent with other studies, the NIRS data collected in this study revealed a slight decrease in [THb] during occlusion, as well as $\%HbO_2$ changes that were characterized by a linear decrease as a function of occlusion duration. Following occlusion, there was an 11-fold increase in blood flow that peaked ~11 s following release of the cuff a recovery and overshoot of [THb] that peaked at ~54 s following cuff release and a recovery and overshoot of $\%HbO_2$ that peaked ~72 s following cuff release. The longer time to peak [THb] is consistent with flow-mediated dilation (FMD), which can occur more than 60 s following the release of the cuff. A higher peak flow during reactive hyperemia was associated with a longer time-to-peak [THb] and a larger increase in [THb] and agrees with previous findings [26,27]. In a clinical setting, a low peak hyperemia and delayed time-to-peak hyperemia indicate reduced FMD and peripheral artery disease; however, the values seen in this study are consistent with healthy young individuals with an ABI in the normal range, as defined in Ref. [29].

It should be noted that absolute quantification of blood flow using U/S is difficult and there are some well-established limitations. For example, although we attempted to include the entire caliber of the popliteal vessel within the sampling gate, this was not always possible. This would result in over estimation of the V_{TAMEAN}. For this reason we have expressed blood flow as a relative change (fold increase) in addition to the more typical absolute changes (ml/min).

Muscle BOLD Contrast at 3T and 7T

Predictably, the R_2* responses to occlusion included an increase in R_2* during occlusion and a decrease in R_2* following occlusion (Table 1). By the end of occlusion, $\%HbO_2$ had dropped from ~70% to ~52%, producing an R_2* increase at 7T that was almost six-fold greater than at 3T. Following occlusion, the $\%HbO_2$ increased from ~70 at rest to ~78%, producing R_2* decreases at both field strengths that were almost two-fold greater at 7T than at 3T. This also is expected to translate to an improved CNR in studies of the post-contraction BOLD response at 7T and a greater dynamic range of responses for the detection of differences among subject groups.

The transverse relaxation properties of blood at 7T differ from those at 3T in several ways. The first is the well-established observation that the R_2* of blood is several-fold greater at 7T than at 3T: for the $\%HbO_2$ values encountered here, the blood R_2* would be expected to range from 150–250 s^{-1} at 7T [17] and from 32–64 s^{-1} at 3T [30]. Another salient difference is that the relationship between blood and tissue R_2* differs for 3T vs. 7T. For all $\%HbO_2$ levels observed, the expected 7T blood R_2* values [17] are uniformly greater than the corresponding muscle R_2* values (Table 1). At 3T the expected blood R_2* value of 32 s^{-1} [30] is lower than the observed muscle value of ~34 s^{-1} at $\%HbO_2$ ~78%. Conversely, for $\%HbO_2$ ~52%, the expected blood R_2* value of 64 s^{-1} [30] is greater than the observed muscle value of ~35 s^{-1}. As noted by Towse *et al*. [8], whether IV BOLD contrast contributes positively or negatively to signal changes will depend on the relative values for

R_2* in muscle and blood. Thus the nature of the IV BOLD contribution to signal (positive or negative) varies with $\%HbO_2$ for 3T studies, but is uniformly negative for 7T studies.

As another consequence of the extremely rapid transverse relaxation of whole blood at 7T, IV BOLD contrast mechanisms are expected to be relatively unimportant at 7T. As a result, EV mechanisms should dominate BOLD contrast. This may explain why the R_2*increased significantly during ischemia at 7T but not at 3T. The progressive increase in R_2* during ischemia at 7T is consistent with a primary, “real time” sensitivity of BOLD phenomena to the microcirculation (which is the site of oxygen transfer from the blood to the tissues). Although we had anticipated larger R_2* changes at 3T [4,10,15,16], there was a large increase in R_2* immediately after the release of the cuff (see Fig. 4). This finding is consistent with IV BOLD effect’s being the predominant source of mBOLD contrast at 3T, as the post-ischemia increase in R_2* would represent the transit of deoxygenated capillary blood to the venous system (the primary site of observation of IV BOLD effects). One particular advantage of this is that with EV BOLD contrast and in the spin-echo condition, a refocusing pulse rephases spins in the vicinity of vessels with diameters greater than ~30 μm [31]. As a result, spin-echo mBOLD signal changes at 7T would be expected to have greater specificity to the muscle microcirculation [31–39], whereas mBOLD contrast changes at 3T reflect a mixed contribution of all unresolved blood vessels. Inasmuch as the microcirculation is a known site of dysfunction in conditions such as obesity [40] and diabetes [41], 7T mBOLD studies may thus afford particular advantages in studies of persons with these conditions.

Conclusions

Muscle BOLD contrast studies are feasible at 7T and result in as much as six-fold greater responses than at 3T. In addition to providing greater SNR and CNR, 7T mBOLD studies may offer further advantages in the form of greater sensitivity to pathological changes to the muscle microcirculation.

Acknowledgments

The authors thank the subjects for their participation and Dr. Amanda Buck, MRI technologists Donna M. Butler, Kristen George-Durrett, Leslie McIntosh, and David Pennell for their assistance with data acquisition. This work was supported by grants from the NIH: R01 AR050101 and UL1 TR000445.

References

1. Lebon V, Brillault-Salvat C, Bloch G, Leroy-Willig A, Carlier PG. Evidence of muscle BOLD effect revealed by simultaneous interleaved gradient-echo NMRI and myoglobin NMRS during leg ischemia. Magn Reson Med. 1998; 40:551–558. [PubMed: 9771572]
2. Toussaint JF, Kwong KK, M’Kparu F, Weisskoff RM, LaRaia PJ, Kantor HL. Interrelationship of oxidative metabolism and local perfusion demonstrated by NMR in human skeletal muscle. J Appl Physiol. 1996; 81:2221–2228. [PubMed: 8941548]
3. Donahue KM, Van Kylen J, Guven S, El-Bershawi A, Luh WM, Bandettini PA, Cox RW, Hyde JS, Kissebah AH. Simultaneous gradient-echo/spin-echo EPI of graded ischemia in human skeletal muscle. J Magn Reson Imaging. 1998; 8:1106–1113. [PubMed: 9786149]
4. Meyer RA, Towse TF, Reid RW, Jayaraman RC, Wiseman RW, McCully KK. BOLD MRI mapping of transient hyperemia in skeletal muscle after single contractions. NMR Biomed. 2004; 17:392–398. [PubMed: 15468084]

5. Towse TF, Slade JM, Meyer RA. Effect of physical activity on MRI-measured blood oxygen level-dependent transients in skeletal muscle after brief contractions. J Appl Physiol. 2005; 99:715–722. [PubMed: 15802369]
6. Damon BM, Hornberger JL, Wadington MC, Lansdown DA, Kent-Braun JA. Dual gradient-echo MRI of post-contraction changes in skeletal muscle blood volume and oxygenation. Magn Reson Med. 2007; 47:670–679. [PubMed: 17390346]
7. Sanchez OA, Louie EA, Copenhaver EA, Damon BM. Repeatability of a dual gradient-recalled echo MRI method for monitoring post-isometric contraction blood volume and oxygenation changes. NMR Biomed. 2009; 22:753–761. [PubMed: 19382156]
8. Towse TF, Slade JM, Ambrose JA, Delano MC, Meyer RA. Quantitative analysis of the post-contractile blood-oxygenation-level-dependent (BOLD) effect in skeletal muscle. J Appl Physiol. 2011; 111:27–39. [PubMed: 21330621]
9. Ledermann HP, Schulte A-C, Heidecker H-G, Aschwanden M, Jager KA, Scheffler K, Steinbrich W, Bilecen D. Blood oxygenation level-dependent magnetic resonance imaging of the skeletal muscle in patients with peripheral arterial occlusive disease. Circulation. 2006; 113:2929–2935. [PubMed: 16785340]
10. Utz W, Jordan J, Niendorf T, Stoffels M, Luft FC, Dietz R, Friedrich MG. Blood oxygen level-dependent MRI of tissue oxygenation: relation to endothelium-dependent and endothelium-independent blood flow changes. Arterioscler Thromb Vasc Biol. 2005; 25:1408–1413. [PubMed: 15890970]
11. Elder CP, Cook RN, Chance MA, Copenhaver EA, Damon BM. Image-based calculation of perfusion and oxyhemoglobin saturation in skeletal muscle during submaximal isometric contractions. Magn Reson Med. 2010; 64:852–861. [PubMed: 20806379]
12. Zheng J, An H, Coggan AR, Zhang X, Bashir A, Muccigrosso D, Peterson LR, Gropler RJ. Noncontrast skeletal muscle oximetry. Magnetic Resonance in Medicine. 2014; 71:318–325. [PubMed: 23424006]
13. Kindig CA, Sexton WL, Fedde MR, Poole DC. Skeletal muscle microcirculatory structure and hemodynamics in diabetes. Respir Physiol. 1998; 111:163–175. [PubMed: 9574868]
14. Mathieu-Costello O. Capillary tortuosity and degree of contraction or extension of skeletal muscles. Microvasc Res. 1987; 33:98–117. [PubMed: 3550394]
15. Damon B, Wadington M, Hornberger J, Lansdown D. Absolute and relative contributions of BOLD effects to the muscle functional MRI signal intensity time course: Effect of exercise intensity. Magn Reson Med. 2007; 58:335–345. [PubMed: 17654591]
16. Sanchez OA, Copenhaver EA, Elder CP, Damon BM. Absence of a significant extravascular contribution to the skeletal muscle BOLD effect at 3T. Magn Reson Med. 2010; 64:527–535. [PubMed: 20665796]
17. Blockley NP, Jiang L, Gardener AG, Ludman CN, Francis ST, Gowland PA. Field strength dependence of R1 and R2* relaxivities of human whole blood to prohance, vasovist, and deoxyhemoglobin. Magnetic Resonance in Medicine. 2008; 60:1313–1320. [PubMed: 19030165]
18. Chang G, Wang L, Cardenas-Blanco A, Schweitzer ME, Recht MP, Regatte RR. Biochemical and physiological MR imaging of skeletal muscle at 7 tesla and above. Seminars in musculoskeletal radiology. 2010; 14:269–278. [PubMed: 20486034]
19. Trattnig S, Zbyn S, Schmitt B, Friedrich K, Juras V, Szomolanyi P, Bogner W. Advanced MR methods at ultra-high field (7 Tesla) for clinical musculoskeletal applications. Eur Radiol. 2012; 22:2338–2346. [PubMed: 22688127]
20. Meyerspeer M, Scheenen T, Schmid AI, Mandl T, Unger E, Moser E. Semi-LASER localized dynamic 31P magnetic resonance spectroscopy in exercising muscle at ultra-high magnetic field. Magnetic Resonance in Medicine. 2011; 65:1207–1215. [PubMed: 21384422]
21. Parasoglou P, Xia D, Chang G, Convit A, Regatte RR. Three-dimensional mapping of the creatine kinase enzyme reaction rate in muscles of the lower leg. NMR in Biomedicine. 2013; 26:1142–1151. [PubMed: 23436474]
22. Kogan F, Haris M, Singh A, Cai K, Debrosse C, Nanga RP, Hariharan H, Reddy R. Method for high-resolution imaging of creatine in vivo using chemical exchange saturation transfer. Magn Reson Med. 2014; 71:164–172. [PubMed: 23412909]

23. Berry KL, Skyrme-Jones RA, Meredith IT. Occlusion cuff position is an important determinant of the time course and magnitude of human brachial artery flow-mediated dilation. Clin Sci (Lond). 2000; 99:261–267. [PubMed: 10995590]
24. Lekakis J, Papamichael C, Vemmos C, Stamatelopoulos K, Voutsas A, Stamatelopoulos S. Effects of Acute Cigarette Smoking on Endothelium-Dependent Arterial Dilatation in Normal Subjects. The American journal of cardiology. 1998; 81:1225–1228. [PubMed: 9604954]
25. Hayoz D, Weber R, Rutschmann B, Darioli R, Burnier M, Waeber B, Brunner HR. Postischemic blood flow response in hypercholesterolemic patients. Hypertension. 1995; 26:497–502. [PubMed: 7649588]
26. Clarkson P, Celermajer DS, Donald AE, Sampson M, Sorensen KE, Adams M, Yue DK, Betteridge DJ, Deanfield JE. Impaired vascular reactivity in insulin-dependent diabetes mellitus is related to disease duration and low density lipoprotein cholesterol levels. J Am Coll Cardiol. 1996; 28:573–579. [PubMed: 8772741]
27. Akre S, Storen G. Relationship between blood flow and vascular volume in skeletal muscle. Scandinavian journal of clinical and laboratory investigation. 1969; 23:115–120. [PubMed: 5372443]
28. Storen G, Akre S. Changes in blood flow and vascular volume in skeletal muscle during reactive hyperemia with free flow or with artificial arterial stenosis. Scandinavian journal of clinical and laboratory investigation. 1969; 23:109–114. [PubMed: 5372442]
29. Aboyans V, Criqui MH, Abraham P, Allison MA, Creager MA, Diehm C, Fowkes FG, Hiatt WR, Jonsson B, Lacroix P, Marin B, McDermott MM, Norgren L, Pande RL, Preux PM, Stoffers HE, Treat-Jacobson D. Measurement and interpretation of the ankle-brachial index: a scientific statement from the American Heart Association. Circulation. 2012; 126:2890–2909. [PubMed: 23159553]
30. Zhao J, Clingman C, Närväinen M, Kauppinen R, van Zijl P. Oxygenation and hematocrit dependence of transverse relaxation rates of blood at 3T. Magnetic Resonance in Medicine. 2007; 58:592–597. [PubMed: 17763354]
31. Kennan RP, Zhong J, Gore JC. Intravascular susceptibility contrast mechanisms in tissues. Magn Reson Med. 1994; 31:9–21. [PubMed: 8121277]
32. Boxerman JL, Hamberg LM, Rosen BR, Weisskoff RM. MR contrast due to intravascular magnetic susceptibility perturbations. Magnetic Resonance in Medicine. 1995; 34:555–566. [PubMed: 8524024]
33. Yacoub E, Shmuel A, Pfeuffer J, Van De Moortele P-F, Adriany G, Andersen P, Vaughan JT, Merkle H, Ugurbil K, Hu X. Imaging brain function in humans at 7 Tesla. Magnetic Resonance in Medicine. 2001; 45:588–594. [PubMed: 11283986]
34. Duong TQ, Yacoub E, Adriany G, Hu X, Uğurbil K, Kim S-G. Microvascular BOLD contribution at 4 and 7 T in the human brain: Gradient-echo and spin-echo fMRI with suppression of blood effects. Magnetic Resonance in Medicine. 2003; 49:1019–1027. [PubMed: 12768579]
35. Yacoub E, Duong TQ, Van De Moortele P-F, Lindquist M, Adriany G, Kim S-G, Uğurbil K, Hu X. Spin-echo fMRI in humans using high spatial resolutions and high magnetic fields. Magnetic Resonance in Medicine. 2003; 49:655–664. [PubMed: 12652536]
36. Yacoub E, Van De Moortele P-F, Shmuel A, Uğurbil K. Signal and noise characteristics of Hahn SE and GE BOLD fMRI at 7 T in humans. Neuroimage. 2005; 24:738–750. [PubMed: 15652309]
37. Zhang N, Yacoub E, Zhu X-H, Ugurbil K, Chen W. Linearity of blood-oxygenation-level dependent signal at microvasculature. Neuroimage. 2009; 48:313–318. [PubMed: 19580875]
38. Uludağ K, Müller-Bierl B, Uğurbil K. An integrative model for neuronal activity-induced signal changes for gradient and spin echo functional imaging. Neuroimage. 2009; 48:150–165. [PubMed: 19481163]
39. Norris DG. Spin-echo fMRI: The poor relation? Neuroimage. 2012; 62:1109–1115. [PubMed: 22245351]
40. Jonk AM, Houben AJHM, de Jongh RT, Serne EH, Schaper NC, Stehouwer CDA. Microvascular dysfunction in obesity: A potential mechanism in the pathogenesis of obesity-associated insulin resistance and hypertension. Physiology. 2007; 22:252–260. [PubMed: 17699878]

41. Fowler MJ. Microvascular and macrovascular complications of diabetes. Clinical Diabetes. 2011; 29:116–122.

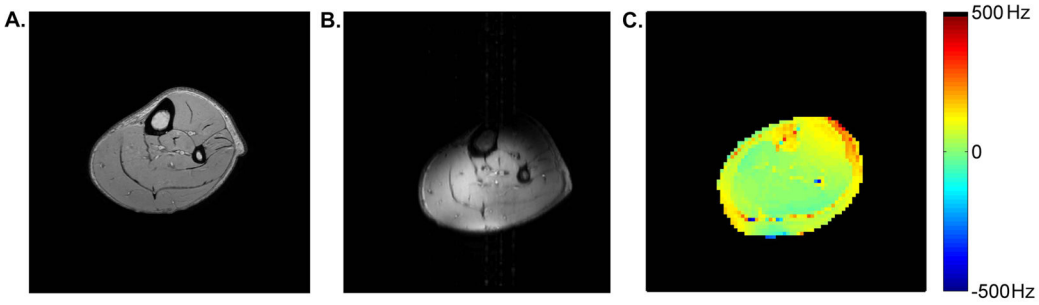

Figure 1.

Sample images from 3T and 7T. Panels **A** and **B** show anatomical images from 3T and 7T, respectively. The 7T anatomical image has substantial signal dropout from the anterior compartment. The images reflect the similarity of axial slice location within the leg. Panel **C** shows a sample ΔB_0 map from 7T. Excluding the chemical shift artifact, the SD of the ΔB_0 map in the poster muscle compartment is 16.4 Hz. All sample data are from this subject.

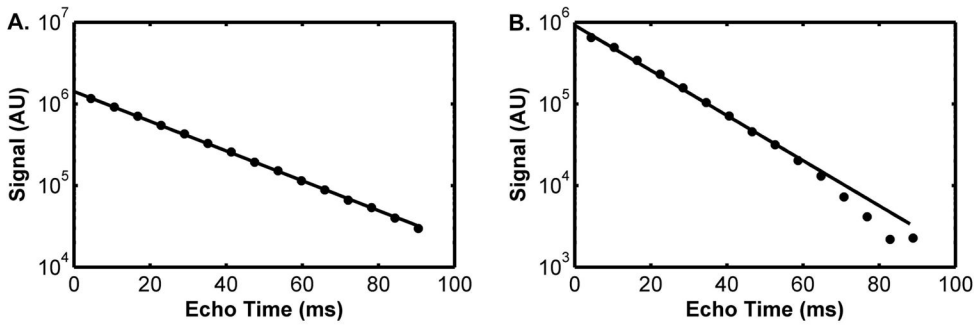

Figure 2.

Sample curve-fitting results from 3T (**A**) and 7T (**B**), from the first pre-occlusion image. The T_2* values corresponding to these data were 23.8 ms (3T) and 15.7 ms (7T). Both plots share the same units on the *y*-axis.

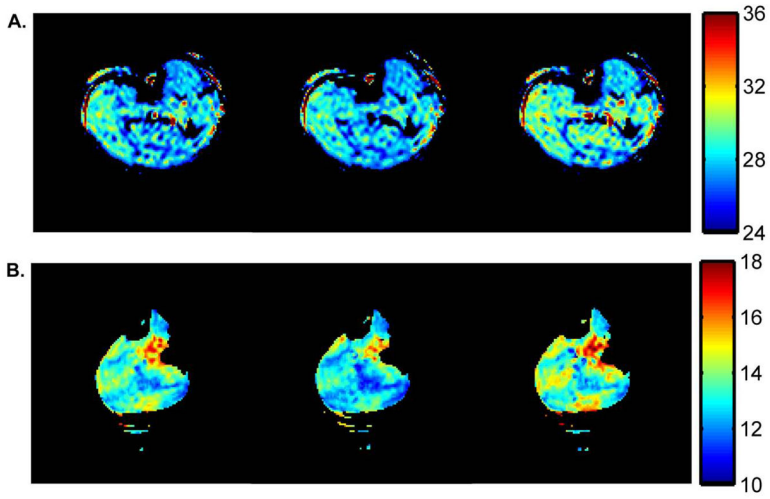

Figure 3.

Sample T_2* maps from 3T (**A**) and 7T (**B**). The T_2* maps reflect the T_2* distribution prior to occlusion (left), at the end of occlusion (middle), and at the time of the peak T_2* value following occlusion (right). The colorbars at right indicate the T_2* in ms. A signal threshold was set so as to exclude curve-fitting in the noise regions of the original images. Due to the sensitivity profile of the partial volume coil used at 7T, this signal threshold also excluded data from areas of low signal in the leg.

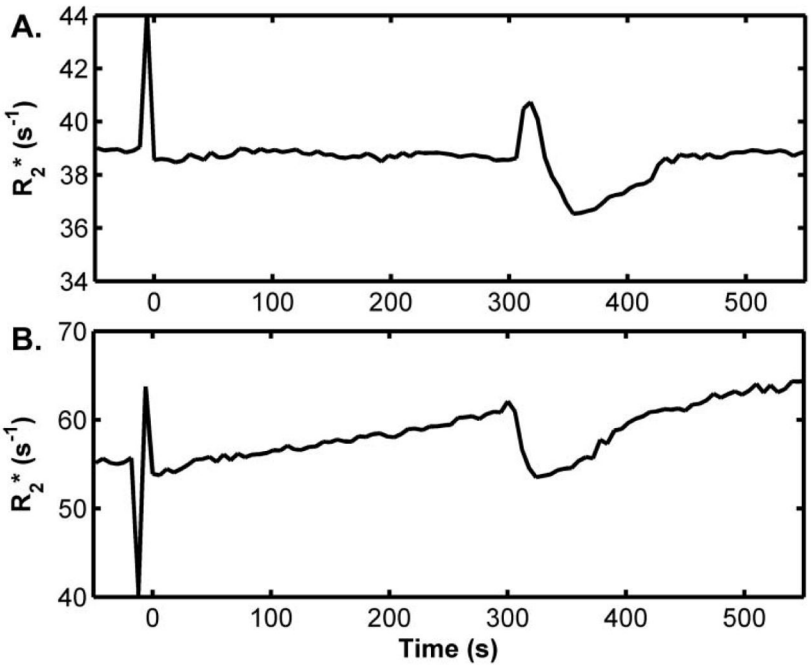

Figure 4.

Sample R_2* time courses from arterial occlusion experiments at 3T (**A**) and 7T (**B**). Time values are referenced to the start of the occlusion period = 0 s and air pressure in the cuff was released at 300 s; both plots share the same time axis.

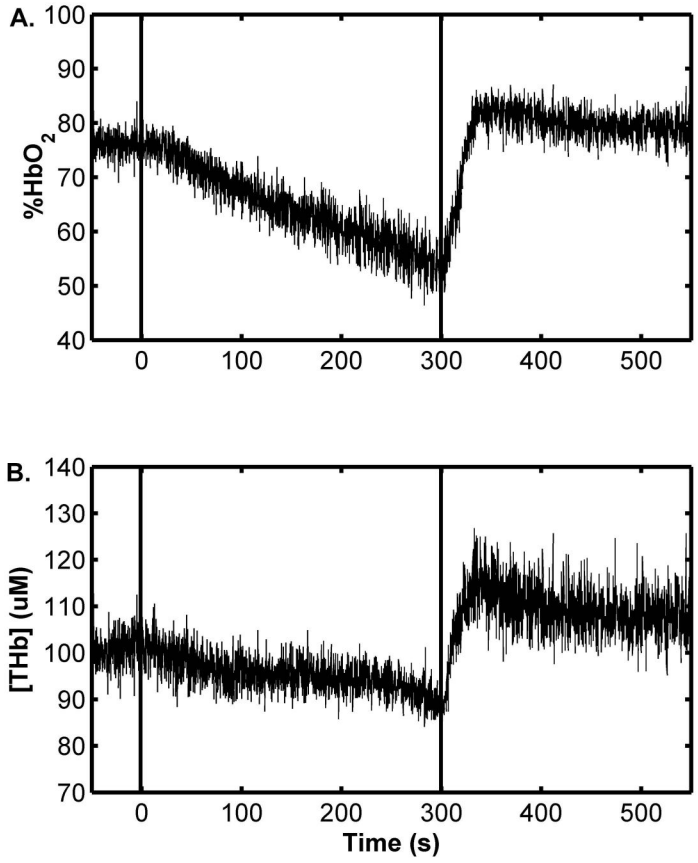

Figure 5.

Sample NIRS data. Data indicate the $\%HbO_2$ (**A**) and [THb] (**B**) time courses from arterial occlusion experiments. Dashed lines indicate the application and the release of the cuff. Time values are referenced to the start of the occlusion period = 0 s; both plots share the same time axis.

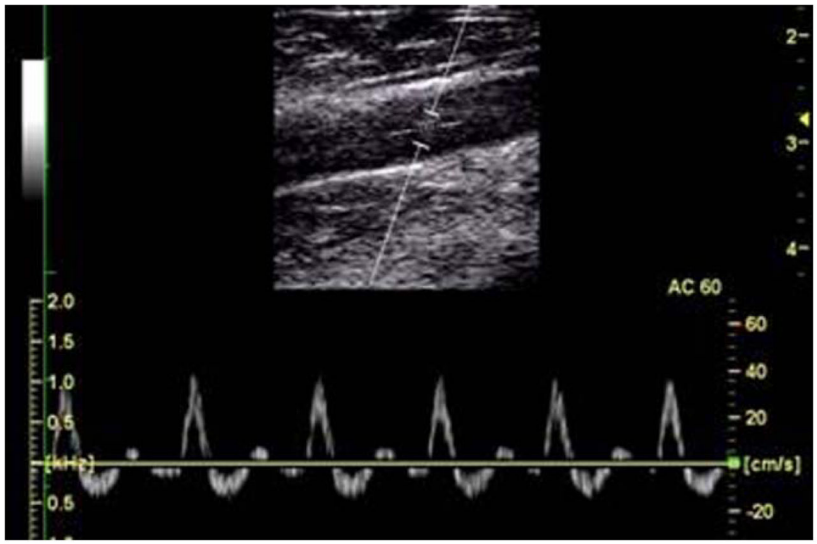

Figure 6.

Sample U/S data, including a B-mode image illustrating the placement of the window in the vessel and PW-mode image showing sample pulse velocity waveforms in the popliteal artery at rest. The tri-phasic waveform is characteristic of the velocity waveform in the peripheral vasculature.

Table 1

R_2* values at 3T and 7T at the pre-occlusion, end-occlusion, and peak post-occlusion time points. Also shown are the time at which the greatest magnitude of post-occlusion T_2* response occurred and the $\Delta R_2{}^*_{END}$ and $\Delta R_2{}^*_{POST}$ values. Mean ± SE are given.

B_0	$R_2{}^*_{PRE}$ (s^{-1})	$R_2{}^*_{END}$ (s^{-1})	$R_2{}^*_{POST}$ (s^{-1})	$\Delta R_2{}^*_{END}$ (s^{-1})	$\Delta R_2{}^*_{POST}$ (s^{-1})
3T	35.17 ± 0.35	36.01 ± 0.38	33.93 ± 0.21	0.84 ± 0.23	−1.24 ± 0.39
7T	60.16* ± 2.95	64.82 ± 2.59	57.80 ± 2.95	4.67* ± 0.63	−2.36* ± 0.25

* Indicates a significant difference between the mean values for 3T and 7T.

Table 2

NIRS-observed values of $\%HbO_2$ and [THb] at the pre-occlusion, end-occlusion, and peak post-occlusion time points. Also shown are the times at which the greatest magnitude of post-occlusion $\%HbO_2$ and [THb] responses occurred, the $\Delta\%HbO_{2END}$ and $\Delta\%HbO_{2POST}$ values, and the $\Delta[THb]_{END}$ and $\Delta[THb]_{POST}$ values. To reduce table size, $\%HbO_2$ and [THb] are replaced with the letter V in the table header; other aspects of the abbreviations are unchanged. Mean ± SE are given; $n = 6$. For the variables reflecting changes from baseline, the 95% CI is also given. None of these CI's included the value zero, indicating statistically significant changes.

V=	V_{PRE}	V_{END}	V_{POST}	$t_{V,POST}$ (s)	ΔV_{END}	ΔV_{POST}
$\%HbO_2$	70.5 ± 1.8	52.7 ± 4.1	78.1 ± 2.7	71.7 ± 15.2	−17.9 ± 4.6 [−29.6, −6.1]	7.6 ± 2.6 [0.9, 14.3]
[THb] (μm)	69.3 ± 14.8	64.9 ± 13.4	79.0 ± 18.3	54.3 ± 9.5	−4.4 ± 0.63 [−8.6, −0.2]	1.6 ± 3.7 [0.1, 19.3]